ELSEVIER

Applied Ocean Research 24 (2002) 83–90

Applied Ocean Research

www.elsevier.com/locate/apor

An experimental study for wave-induced instability of pipelines: the breakout of pipelines

F.P. Gao[a,1,2], X.Y. Gu[b], D.S. Jeng[a,*], H.T. Teo[a]

[a]*School of Engineering, Griffith University Gold Coast Campus, Parkwood, QLD 9726, Australia*
[b]*Institute of Mechanics, Chinese Academy of Sciences, Beijing 100080, People's Republic of China*

Received 10 January 2002; revised 7 June 2002; accepted 10 June 2002

Abstract

In this paper, a series of experiments have been conducted in a U-shaped oscillatory flow tunnel, which provides a more realistic simulation than the previous actuator loading methods. Based on the experimental data of pipe displacement with two different constraint conditions (freely laid pipelines and anti-rolling pipelines), three characteristic times in the process of pipeline losing stability are identified. The effects of sand size on the pipeline lateral stability are examined for freely laid pipelines. The empirical relationships between non-dimensional pipeline weight (G) and Froude number (Fr_b) are established for different constraint conditions, which will provide a guide for engineering practice.

Keywords: Pipeline breakout; Lateral instability; Oscillatory flow; Sandy seabed; Wave loading; Submarine pipeline

1. Introduction

Wave-induced lateral instability of untrenched submarine pipeline is a wave–pipe–seabed coupling problem. Under wave loading, to limit the lateral movement of untrenched pipeline, a balance exists between wave loading, the submerged weight of pipeline and soil resistance. Without sufficient resistance from the soil, breaking of pipeline will occur as a result of pipeline instability [1]. Conventionally, to avoid the occurrence of such instability, the pipeline has to be given a heavy weight coating or alternatively be anchored/trenched into the soil to avoid the occurrence of pipeline instability. Since both methodologies are considered expensive and complicated from the aspects of design and construction. Therefore, the study on wave-pipe–soil interaction problem regarding the stability of pipelines is particularly important for coastal engineers involved in the design of pipelines.

In the past decades, with the increasing demand for submarine pipelines to transport natural oil and gas, many researchers had focused particularly on solving wave-induced pipeline instability problems [1–4]. However, this problem has not been fully understood because of the complicated soil behavior and geometry of pipelines [5]. Numerous experimental studies on the lateral stability of untrenched pipelines have been carried out with cyclic actuator loading methods since the 1980s [2–4]. Among these, Wagner et al. [2] improved the Coulomb friction theory into an empirical pipe–soil interaction model, in which the total lateral resistance was assumed to be the sum of the Coulomb friction component and the soil passive resistance component. Brennoden et al. [3] further proposed an energy-based pipe–soil interaction model, in which the soil passive resistance component is related to the work done by pipe during its movement. It has been reported that remarkable cost benefits can be achieved by reduction of designed weight of pipe, when considering the soil passive resistance [4]. The aforementioned studies indicated that the traditional design method based on the Coulomb friction theory was too conservative. However, in the above experimental investigations, the wave loads were not modeled with hydrodynamic methods but exerted with mechanical actuators, and no water was filled in the tank. Therefore, the wave-induced sand scour around the pipeline could not be modeled properly. The wave-induced oscillatory flow around the pipeline does not only affect the

* Corresponding author. Tel.: +61-7-5552-8683; fax: +61-7-5552-8065.
E-mail address: d.jeng@mailbox.gu.edu.au (D.S. Jeng).
[1] On leave from Institute of Mechanics, Chinese Academy of Sciences, Beijing, People's Republic of China.
[2] Current address: Centre for Offshore Foundation Systems, The University of Western Australia, Nedlands, WA 6009, Australia.

0141-1187/02/$ - see front matter
PII: S0141-1187(02)00012-3

Nomenclature

A	displacement of the oscillatory flow
A_0	amplitude of flow displacement
$\dot{A}_0$	velocity of the increase of oscillatory flow amplitude
C_u	uniformity coefficient
D_r	relative density of sand
d_s	sand diameter
d_{10}	grain size at which 10% of the soil weight is finer
d_{50}	mean grain size of sand
e_0	initial void ratio
Fr	Froude number, $Fr = U_m/\sqrt{gD}$
g	gravitational acceleration
KC	Keulegan–Carpenter number, $KC = U_m T/D$
m	parameter for the model
p	parameter for the prototype
Re	Reynolds number, $Re = U_m D/\nu$
T	wave period
t	total loading time
t_s	the time when sand bed beside the pipe is scoured
t_r	the time when pipe begins to move slightly (the movement of pipe is detectable)
t_b	the time when pipe breakouts from its original site, i.e. pipe looses lateral stability
U_m	maximum value of the velocity of water particles at seabed
W_s	submerged weight of pipeline
ρ_{sat}	density of saturated sand
ρ_w	density of water
γ'	the buoyant unit weight of soil
γ	unit weight of saturated sand
γ_d	dry unit weight
λ	ratio of the parameters of model to prototype
ω	frequency of oscillatory flow, $\omega = 2\pi/T$

pipeline but also the seabed. In general, the on-bottom stability of the submarine pipeline is the problem of interaction between wave, soil and pipe, rather than only the pipe–soil interaction under cyclic loading as considered in the previous works.

Numerous hydrodynamic experiments have been conducted to investigate scour under fixed pipelines in the past [1,6]. For example, Stansby and Starr [6] studied the wave-induced settlement of pipeline. Nevertheless, the horizontal movements were not allowed in their experiments. Thus, the phenomena of on-bottom stability could not be really reflected. On the other hand, Foda et al. [1] examined the vertical stability of half-buried pipe with wave flume, which no scour was observed in their experiments. Since the flow characteristics around half-buried pipeline is different from that around untrenched pipeline. In fact, from the aspect of wave–pipe–soil interaction, the breakout of untrenched pipeline is more complicated than that of half-buried one. To date, no experimental data regarding the lateral stability of untrenched pipeline is yet available.

The aim of this paper is to provide a better understanding of the physics of lateral stability or breakout of untrenched offshore pipelines under wave loading. To achieve this, hydrodynamic loading method is adopted. Based on the experimental results, the empirical formulas for the prediction of the instability of both freely laid pipelines and anti-rolling pipelines will be established, respectively.

2. Dynamic simulation of the wave–seabed–pipe interaction

In the field, the storm wave events are unpredictable and the field conditions are often characterized with significant uncertainty. Thus, development and testing of offshore pipeline model in laboratory is essential, for it is difficult to accurately obtain data from prototypes. However, care must be taken to make sure that the model simulates the behavior of the prototype as accurately as possible.

The similarity method proposed by Chakrabarti [7] can be utilized for modeling wave-induced breakout of untrenched submarine pipelines, which is a 'wave–pipeline–soil' coupling problem, and thereby, the properties of wave, pipeline and soil are involved. The critical submerged weight of pipeline per meter to keep itself stable, W_s, is mainly related to the following parameters

$$W_s = f(D, \kappa, T, U_m, \nu, t, \dot{A}_0, \rho_{sat}, \rho_w, g, d_s, D_r), \quad (1)$$

where D is the pipe diameter, κ the roughness coefficient of pipe surface, T the wave period, U_m the maximum value of the velocity of water particles at seabed, ν the kinematics viscosity of water, t the total loading time, $\dot{A}_0$ the velocity of the increase of oscillatory flow amplitude, ρ_{sat} the density of saturated sand, ρ_w the density of water, g the gravitational acceleration, d_s the sand diameter and D_r is the relative density of sand.

Based on Vaschy–Buckinghan's theorem, ten independent dimensionless parameters can be obtained from Eq. (1). A functional relationship that represents the phenomenon of pipeline instability may be expressed as

$$G = \frac{W_s}{\gamma' D^2} = F\left(Fr, \mathrm{KC}, Re, \frac{t}{T}, \frac{\dot{A}_0}{U_m}, \frac{\rho_{sat}}{\rho_w}, \frac{D}{d_s}, D_r, \kappa\right), \quad (2)$$

where the dimensionless submerged weight of the pipeline, G, is defined as $G = W_s/(\gamma' D^2)$ (in which $\gamma' = (\rho_{sat} - \rho_w)g$ is the buoyant unit weight of soil). Froude number, Fr, is

defined as $Fr = U_m/\sqrt{gD}$, while Reynolds number, Re, is given by $Re = U_m D/\nu$.

In Eq. (2), the Keulegan–Carpenter number, KC, is defined as $KC = U_m T/D$. In general, KC number controls the generation and development of vortex around pipeline under oscillatory flow loading [8]. Also, it is related to the hydrodynamic force on the pipe under wave action.

Based on above similarity analysis, the dimensionless parameters in Eq. (2) can be deduced to three important parameters, Froude number (Fr), Keulegan–Carpenter number (KC) and Reynolds number (Re), which are relevant to flow characteristics.

According to principle of similarity, we can obtain the following relationship from Froude number

$$\lambda_{U_m} = \lambda_D^{1/2}, \tag{3}$$

where λ represents the ratio of the parameters of model to that of prototype. Eq. (3) further renders to

$$\lambda_T = \frac{\lambda_D}{\lambda_{U_m}} = \lambda_D^{1/2}. \tag{4}$$

Based on Eq. (4) and the definition of KC number, we have

$$\lambda_{KC} = \frac{\lambda_{U_m}\lambda_T}{\lambda_D} = 1. \tag{5}$$

This indicates that Fr and KC numbers can be satisfied concurrently in the model tests. However, if the quantities strongly depend on Reynolds number, direct scaling is not possible. In the case of water wave with a free surface, the gravitational effect predominates, and pipeline on-bottom stability is related to the submerged weight of the pipeline. The effect of other factors, such as viscosity, surface tension, etc., is generally small and negligible. Since both Fr and Re cannot be satisfied concurrently for model tests, it is convenient to employ the Froude scaling process and allowance are made for variation in Reynolds number. For example, the values of Fr and KC numbers of coastal sediments in South China Sea vary between 0–0.5 and 0–20, respectively, which is the range we used in the laboratory experiments. However, the Re number is smaller than the actual value by about two orders.

3. Experiment set-up

3.1. U-shaped oscillatory water flow tunnel

When gravitational ocean waves propagate over the shallow ocean zone, the water particles oscillate elliptically at upper water level with certain frequency, but mainly horizontally near the sea bottom due to the boundary effect, as sketched in Fig. 1. The oscillatory flow induces drag, inertia and lift forces upon the pipeline, which will affect the pipeline lateral stability. For simulating the oscillation of water particles near the seabed, a U-shaped oscillatory flow

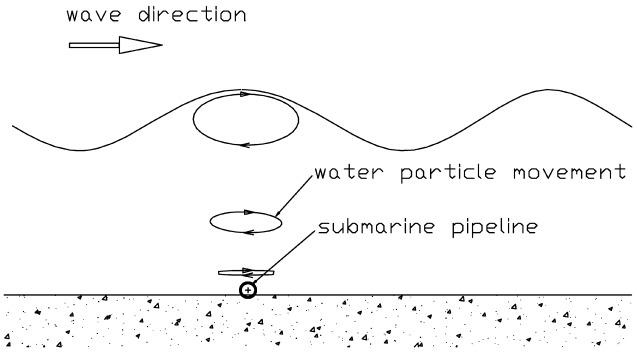

Fig. 1. Schematic diagram of a harmonic wave passing over a pipeline.

water tunnel is employed, as shown in Fig. 2(a). The water tunnel is made of apparent plexiglass with section area of $0.2 \times 0.2\ m^2$. By the periodical opening and closing of the butterfly-valve on top of one limb of the water tunnel, the inner water can accomplish a simple harmonic oscillation

$$A = A_0(t)\sin \omega t, \tag{6}$$

where A is the displacement of the oscillatory flow, A_0 the amplitude of flow displacement, ω the frequency of oscillatory flow, i.e. $\omega = 2\pi/T$, T (= 2.60 s) the inherent period of the oscillatory flow, and t is the loading time. The amplitude of the oscillatory flow $A_0(t)$ can be varied continuously from zero up to 200 mm by means of

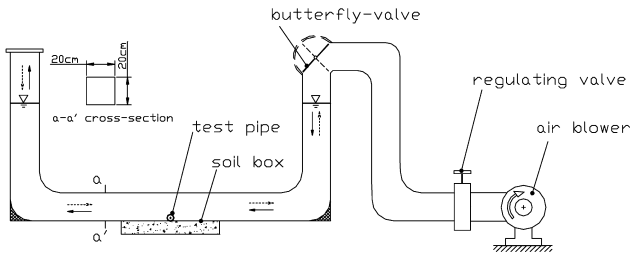

(a)

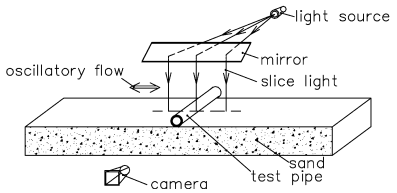

(b)

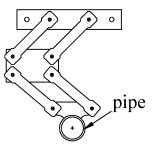

(c)

Fig. 2. Experiment set-up: (a) U-shaped oscillatory water flow tunnel, (b) schematic diagram of test observation, (c) pipeline anti-rolling device.

regulating valve to change the effective air flux from air blower.

The lower part of the water tunnel constitutes the test section, under which a soil box with length of 0.60 m, width of 0.20 m, depth of 0.035 m is constructed. The soil box, which is mainly filled with sand, is used as the model for sandy seabed.

Since the main predominance of the U-tube experiment is its ability of modeling the horizontal movement of water particles, which is one of the main factors cause scouring and pipe instability. The dynamic pressure induced by waves could not be modeled in U-tube. However, the scale of the wave dynamic pressure is much smaller than static pressure in the small scale model test. Thus, we use the horizontal movement of the water particle to represent the horizontal wave loading on the whole wave–soil–pipe interaction problem.

3.2. Pipeline model

3.2.1. Two constraint conditions

As to a long distance laid pipeline, the stability of pipeline at separate sections is different. For example, the demands for the stability of pipeline sections near risers, are higher than that of normal ones. Due to the constraints from risers and pipeline's own anti-torsion rigidity, pipeline movement is not purely either horizontal or rotational. In the previous actuator loading experiments [2–4], only the stability of anti-rolling pipes was studied. Here, we consider the following two constraint conditions:

(1) Case I: pipeline is free at its ends (Fig. 2(b));
(2) Case II: the rolling of the pipeline is restricted, but pipeline can move freely in horizontal and vertical directions. A device for anti-rolling of pipeline was designed, as shown in Fig. 2(c). The anti-rolling device is mainly made of mini bearings and thin plexiglass plate, whose density is nearly same as that of water, therefore, it does not lay additional resistance on pipe section but only provides anti-rolling torsion while pipe moving. The device includes two parts, which are installed at the two ends of the pipeline separately.

3.2.2. Submerged weight of pipelines

The submerged weight of pipeline is the main concern for the on-bottom stability design. The effects of submerged weight of pipelines with different outer diameters on pipeline instability are studied in the paper.

According to the similarity parameter G in Eq. (3), the submerged weight of test pipes can be adjusted to model the typical submerged weight of actual pipelines. The parameter G for the model and prototype pipes can also be expressed as

$$G = \frac{(W_s)_p}{\gamma_p D_p^2} = \frac{(W_s)_m}{\gamma_m D_m^2}, \tag{7}$$

where the subscripts 'p' and 'm' represent the parameters for the prototype and model, respectively. Referring to the typical $(W_s)_p$ of actual pipes with diameter of 1.0 m, which is from about 1.0–3.0 kN/m [2,3], leading to the values of G varying between 0.1 and 0.3.

The submarine pipeline generally has a large span so that the wave-induced breakout of pipeline may be treated as a two-dimension problem. The model pipe spans the soil box vertically to the direction of oscillatory flow, as shown in Fig. 2(a). In the experiments, to minimize the ending effects, the test pipes composed of aluminium have the length of 0.19 m, thus the gaps between pipe ends and the U-shaped tunnel side walls are about 5 mm. Thereby, local scouring at the end of the pipe model is not considered as a problem, which has been proved in the experiments.

3.3. Test materials

Because of the proximity of the pipeline to the seafloor, the modeling of soil characteristic of the foundation is important. Two kinds of sand are used, i.e. medium sand and fine sand, whose index properties are shown in Table 1, where d_{50} is the mean grain size of sand, d_{10} the grain size at which 10% of the soil weight is finer, C_u the uniformity coefficient, γ the unit weight of saturated sand, γ_d is the dry unit weight, e_0 the initial void ratio and D_r is sand relative density. The difference of the unit weights of test sand in different tests is controlled within an error of 5%.

The moist sand is firstly saturated, then packed in the soil box under water, and finally, trimmed flat with a scraper. Afterwards, the pipe is laid on surface of the flat sandy bed. There always exists an initial embedment, the magnitude of which is dependent on the properties of pipe and soil. Conventionally, the ratio of initial embedment to the pipe diameter varies between 0.03 and 0.05.

3.4. Procedure of experiments

To explore the mechanism of pipeline lateral instability induced by rapidly increasing storm wave, a constant velocity of the increase of oscillatory flow amplitude, i.e. $\dot{A}_0 \approx 9 \times 10^{-5}$ m/s, is adopted in the experiments.

From Eq. (10), the velocity of oscillatory flow $U(t)$ can be deduced as

$$U(t) = \dot{A}_0(t)\sin \omega t + \omega A_0 \cos \omega t. \tag{8}$$

In the experiments, $A_0(t)$ is the order of 10^{-1} (m), thus, $\dot{A}_0/(\omega A_0) \approx 0(10^{-3})$. Therefore, the maximum water

Table 1
Index properties of the test sands

Sand type	d_{50} (mm)	d_{10} (mm)	C_u	γ (kN/m^3)	γ_d (kN/m^3)	e_0	D_r
Medium sand	0.38	0.30	1.4	19.00	14.80	0.73	0.37
Fine sand	0.21	0.11	2.0	21.05	17.47	0.56	0.60

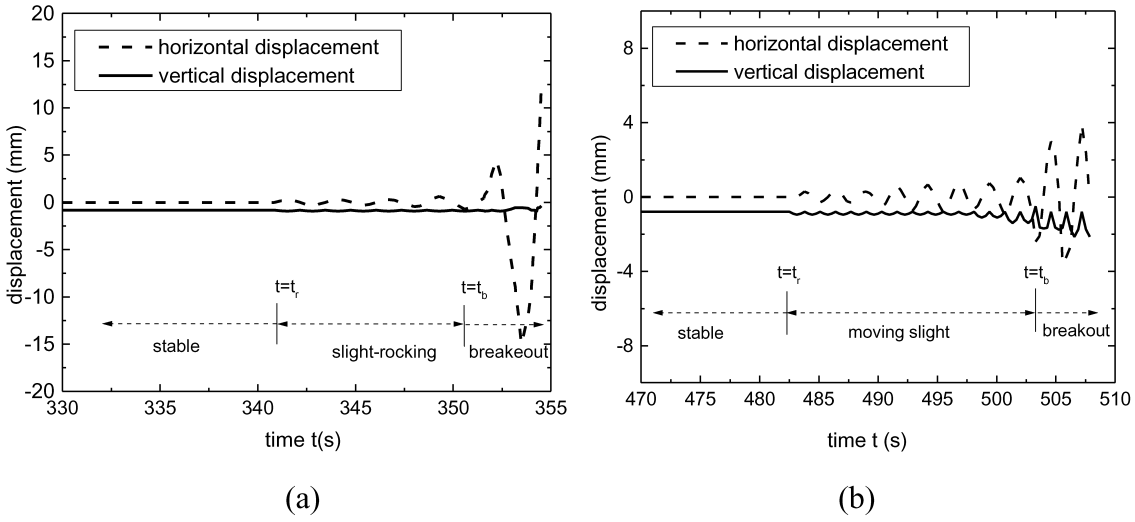

Fig. 3. The distribution of the displacement of pipeline versus time for (a) freely laid pipe (Test No. 2) and (b) anti-rolling pipe (Test No. 3).

particle velocity of the oscillating flow U_m is as follows:

$$U_m \approx \omega A_0(t). \tag{9}$$

During the experiments, the change of water level was recorded with a set of differential pressure transducers and data acquisition system. To find the commencing condition of sand scour, sand scour visualization was carried out under the sliced light by a video camera. Meanwhile, the instability process of the pipe was also observed and recorded by the video camera, as shown in Fig. 2(b).

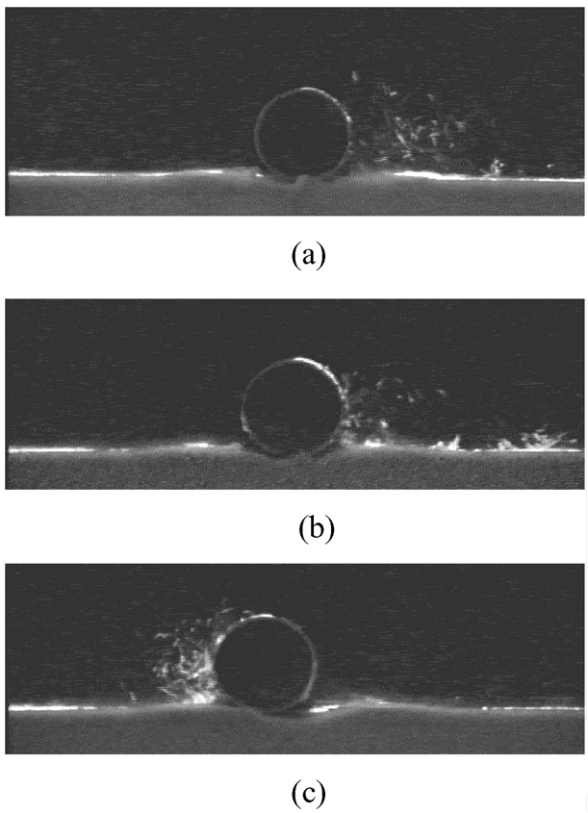

Fig. 4. Three characteristic states of pipe instability (Case I). (a) Onset of sand scour, (b) pipeline rocks, and (c) pipeline breakouts.

4. Experiment results

4.1. The phenomena of pipeline instability

4.1.1. Characteristic times

With the increase of A_0, the displacements of pipes in the horizontal and vertical directions in Cases I and II are shown in Fig. 3. Three characteristic times in pipeline instability process can be identified as

(1) $t = t_s$: at a certain distance apart from the pipe, the sand grains at the bed surface start to move visibly. Onset of scour occurs (Fig. 4(a));
(2) $t = t_r$: the pipe moves slightly (Fig. 4(b));
(3) $t = t_b$: the pipe breakout from original site (Fig. 4(c)).

4.1.2. Phases of pipeline instability process

Correspondingly, the pipe and the surrounding sandy bed experience four typical phases:

(1) Totally stable phase ($t < t_s$) : the pipeline is stable completely.
(2) Metastable phase ($t_s \le t < t_r$) : when the flow velocity is large enough to create considerable amount of sediment in suspension, it forms the main contribution to the sediment transport and piles up in the outer directions. Sand ripples are gradually formed in the vicinity of the pipe (Fig. 4(a))
(3) Pre-failure phase ($t_r \le t < t_b$) : at $t = t_r$, the pipe begins to move slightly in the horizontal and vertical directions (Figs. 3 and 4(b)).
(4) Breakout phase ($t \ge t_b$) : at $t = t_b$, the pipe suddenly

moves away from its original site, or breakout takes place, after a period of slight moving (Fig. 4(c)).

4.1.3. Comparison of pipeline instability phenomena for different constraint conditions

In general, the process of pipeline instability includes the aforementioned four phases during instability process. For both constraint cases, the phenomena are similar in the first and second phases. This indicates that constraint condition does not affect the regularity of sand scouring. However, the influence of constraint condition on the sand scouring is observed in the third and fourth phases. For example, in the third phase, the freely laid pipe (Case I) rocks at the same frequency with that of oscillatory flow, and its bottom keeps contacting sand bed during this period. On the other hand, as for the anti-rolling pipeline (Case II), it moves in horizontal direction at the range of about 1–3% of D, accompanied by a slight settlement less than 1% of D (Fig. 3). In the fourth phase, the freely laid pipeline rolls over the dune nearby from its original site in a sudden (Fig. 4(c)). However, the anti-rolling pipeline moves horizontally at the distance about 20–30% of D, pushing the sand piled up nearby (Fig. 5).

The instability process of pipes with same diameter of 0.030 m and various submerged weights are shown in Fig. 6. The figure shows that the erosion occurs at the same flow velocity for both the kinds of pipes. Furthermore, the weight of the pipeline has no effect on the onset of erosion, which implies that the water particle velocity is the main cause of the onset of sand scour. The instability of pipeline is always accompanied with sand scouring, which was not revealed in the earlier experiments [2–4]. However, as to the pipelines whose submerged weights are small, such as Test No. 1, the pipeline breakouts when the oscillatory flow is insufficient to cause sand scour.

4.2. Criterion for the on-bottom instability of pipeline

In the experiments, numerous pipe diameters are used for different cases. For example, $D = 0.014$, 0.02 and 0.03 m are used for medium sand, while $D = 0.02$ and 0.03 m are used for fine sand. The oscillatory flow amplitudes at which pipe looses stability ($A_0 = A_b$) were recorded. The corresponding KC and Fr numbers, named as KC_b and Fr_b, can

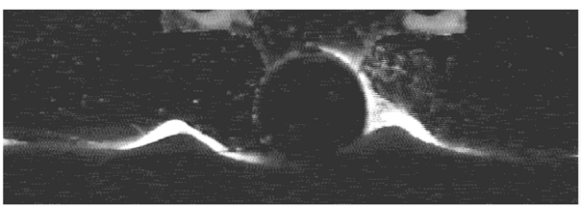

Fig. 5. Phenomena of pipe losing stability (Case II).

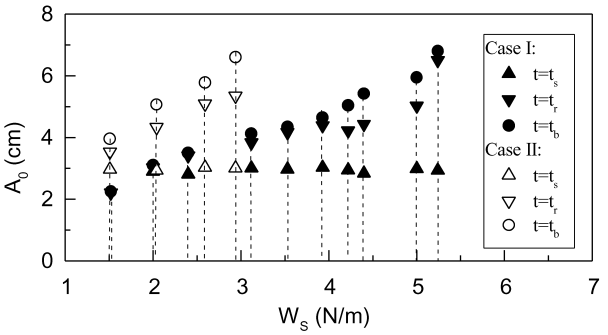

Fig. 6. Instability process for pipes with different weight ($D = 0.030$ m, medium sand).

be obtained as

$$KC_b = \frac{2\pi A_b}{D} \quad \text{and} \quad Fr_b = \frac{2\pi A_b}{T\sqrt{gD}}. \tag{10}$$

The experiment results for all cases are tabulated in Table 2.

Table 2
Experimental data (Case I in medium sand: Test No. 1–19; Case I in fine sand: Test No. 20–29; Case II in medium sand: Test No. 30–37)

Test No.	D (m)	W_s (N/m)	γ' (N/m^3)	G	A_b (cm)	KC_b	Fr_b
1	0.030	1.52	9.0×10^3	0.188	2.21	4.62	0.099
2	0.030	2.00	9.0×10^3	0.247	3.11	6.51	0.139
3	0.030	2.40	9.0×10^3	0.296	3.51	7.35	0.157
4	0.030	3.12	9.0×10^3	0.385	4.14	8.67	0.185
5	0.030	3.53	9.0×10^3	0.436	4.37	9.14	0.195
6	0.030	3.93	9.0×10^3	0.485	4.66	9.76	0.208
7	0.030	4.22	9.0×10^3	0.521	5.05	10.58	0.226
8	0.030	4.40	9.0×10^3	0.543	5.44	11.38	0.243
9	0.030	5.00	9.0×10^3	0.617	5.97	12.50	0.267
10	0.030	5.24	9.0×10^3	0.647	6.80	14.24	0.304
11	0.020	1.09	9.0×10^3	0.303	3.08	9.68	0.169
12	0.020	1.35	9.0×10^3	0.375	3.60	11.30	0.197
13	0.020	1.54	9.0×10^3	0.428	3.82	12.00	0.209
14	0.020	1.72	9.0×10^3	0.478	4.01	12.60	0.220
15	0.020	1.97	9.0×10^3	0.547	4.81	15.10	0.263
16	0.014	0.78	9.0×10^3	0.442	3.41	15.30	0.223
17	0.014	0.89	9.0×10^3	0.505	3.48	15.60	0.228
18	0.014	1.05	9.0×10^3	0.595	3.95	17.71	0.258
19	0.014	1.21	9.0×10^3	0.686	5.31	23.82	0.347
20	0.030	1.61	11.1×10^3	0.162	2.03	4.24	0.091
21	0.030	2.00	11.1×10^3	0.201	3.26	6.82	0.146
22	0.030	2.40	11.1×10^3	0.241	3.45	7.22	0.154
23	0.030	3.12	11.1×10^3	0.314	3.87	8.11	0.173
24	0.030	3.53	11.1×10^3	0.355	4.54	9.51	0.203
25	0.030	3.93	11.1×10^3	0.395	4.68	9.79	0.209
26	0.030	4.22	11.1×10^3	0.424	5.75	12.03	0.257
27	0.030	4.50	11.1×10^3	0.452	5.96	12.47	0.266
28	0.030	5.00	11.1×10^3	0.503	6.32	13.23	0.283
29	0.030	5.29	11.1×10^3	0.532	6.92	14.49	0.310
30	0.030	1.51	9.0×10^3	0.186	3.97	8.31	0.178
31	0.030	2.04	9.0×10^3	0.252	4.99	10.44	0.223
32	0.030	2.59	9.0×10^3	0.320	5.79	12.12	0.259
33	0.030	2.94	9.0×10^3	0.363	6.61	13.84	0.296
34	0.020	0.78	9.0×10^3	0.217	3.87	12.14	0.212
35	0.020	0.98	9.0×10^3	0.272	4.52	14.19	0.248
36	0.020	1.12	9.0×10^3	0.311	4.79	15.04	0.262
37	0.020	1.29	9.0×10^3	0.358	5.33	16.74	0.292

Based on values of W_s, D and γ', the non-dimensional pipe submerged weight G can then be calculated, as shown in Table 2.

4.2.1. Freely laid pipeline

Fig. 7 shows the correlation between Fr_b and G for Case I in medium sand (the solid line), which is also listed in Table 2 (Test No. 1–19). With regards to the same sand, all the data for different pipe diameters fall within the range with an approximately linear relationship. Although a regression polynomial could be well fitted within the same error margin as the linear approximation, we use a linear relation for its simplicity in practical applications. Due to that the effects of pipeline diameter are not involved in the relationship between Fr_b and G, this provides the possibility of applying them for a reference in practical design. For simplicity in practical applications, the least square fitting equation of the experimental data for Case I in medium sand is given as

$$Fr_b = 0.042 + 0.38G \qquad (0.18 < G < 0.65). \tag{11}$$

This correlation describes the critical state of breakout or lateral instability of freely laid pipelines. The above results coincide with the conclusions drawn by Chakrabarti [7] and Poorooshasb [9].

To explore the effects of sand properties on pipeline instability, experiments on fine sand were conducted. The properties of testing materials are listed in Table 1. The pipes with diameter $D = 0.030$ m and with different submerged weights W_s were adopted in these experiments. The results for Case I in fine sand are listed in Table 2 (Test No. 20–29). The correlation between Fr_b and G in fine sand is presented in Fig. 7 as a dashed line, which also shows that an approximately linear relationship exists between the two

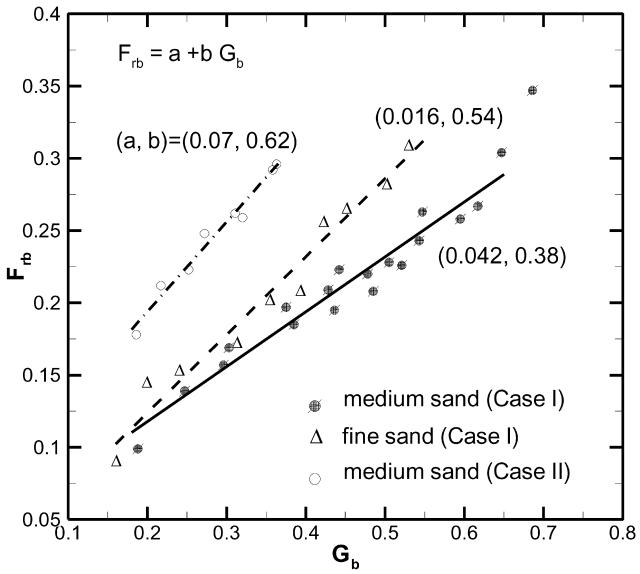

Fig. 7. Relationship between Fr_b and G. Solid line: medium sand (Case I), dashed line: fine sand (Case I), and dashed-dotted line: medium sand (Case II).

non-dimensional parameters, within the given range of G_b, which can be expressed as

$$Fr_b = 0.016 + 0.54G \qquad (0.16 < G < 0.55). \tag{12}$$

Fig. 7 clearly demonstrates the effects of soil properties on the pipeline stability. For example, with same dimensionless parameter, Fr_b, which represents the loading, the value of G to keep pipeline stable on medium sand is greater than that on fine sand. This can also be explained by the consideration of the penetration of the pipe. For pipeline directly laid upon the seabed, natural settlement will occur. As observed in the experiment, the natural settlement in fine sand is greater than that in medium sand, which provides addition resistance. Thus, a smaller G value is required in fine sand when compared with medium sand for a given Fr_b value.

4.2.2. Anti-rolling pipeline

By means of the designed anti-rolling device, as shown in Fig. 2(c), experiments were conducted on medium sand for pipelines with different diameters, such as $D = 0.03$ and 0.02 m, as well as with different submerged weight. Similar to the experiments on freely laid pipelines, the oscillatory flow amplitude also rises at the same speed $\dot{A}_0$. The experimental results of Case II are listed in Table 2 (Test No. 30–37).

The correlation between Fr_b and G for Case II in medium sand is also included in Fig. 7 (the dashed-dotted line). Similar to the results in Case I, all the experimental data with different pipe diameters fall within the range with an approximately linear relationship. The fitting formula between Fr_b and G with least square method is given for Case II, as follows

$$Fr_b = 0.069 + 0.62G \qquad (0.18 < G < 0.36). \tag{13}$$

This correlation describes the critical state of lateral instability of anti-rolling pipelines.

4.2.3. Comparison between two constraints

The linear Fr_b–G relations can be summarized in an empirical formula as

$$Fr_b = a + bG. \tag{14}$$

The comparison of Fr_b–G curves between two constraint conditions, i.e. Cases I and II, in medium sand is presented in Fig. 7. The figure indicates that

(1) With same submerged weight of pipeline, G, the critical Fr_b, at which lateral instability for anti-rolling pipeline occurs, is much higher than that for freely laid pipeline, as expected.
(2) The slope of Fr_b–G curve for anti-rolling constraint is larger than that for freely laid constraint.

Based on the above analysis, it is obvious that the stability of anti-rolling pipelines is obviously higher than that of freely laid pipelines. The anti-rolling device appears

to provide additional resistance from the pipe and sand interactions, for which the resting pipe on the sand will dig itself deeper when being pushed horizontally (Fig. 2(b) and (c)). Thus, the free laid pipe test is more representative of actual instability. Most of the earlier actuator experiments [2–4], in which only anti-rolling pipes were concerned, are not suitable for the long laid submarine pipeline, in which constraint condition should be closer to Case I than to Case II.

5. Conclusions

Based on the analysis of a series of experiments conducted in an oscillatory flow tunnel, the following conclusions can be drawn:

(1) Three characteristic times in process of pipe lateral instability, i.e. (a) onset of sand scour, (b) pipe rocking, (c) pipe breakout, are revealed from the pipe displacements records and experimental observation.
(2) By means of dimensional analysis, the linear relationships between the pipe weight parameter G and hydrodynamic parameters Fr_b have been obtained. A comparison has been made between freely laid pipelines and anti-rolling pipelines. As expected, the anti-rolling pipes are significantly more stable than freely laid pipes. The critical $Fr_b - G$ lines could serve as a supplementary analysis for practical pipeline on-bottom stability design.
(3) The effects of sand properties are examined for freely laid pipes. It indicates that the sand particle size has influence on soil permeability and sediment scour around pipes, which will eventually affect pipeline lateral instability.
(4) The lateral instability of untrenched pipeline is always coupled with the sand scouring and pore water seepage. The hydrodynamic experiments reflect the coupling effects of 'wave–pipe–soil' interaction much more than the earlier actuator tests.

Acknowledgments

This study was jointly supported by the Chinese National Scientific Foundation Projects (19772057) and the key project of the Ninth 5-year Plan of Chinese Academy of Sciences (KZ951-A1-405-01). This work was also partially supported by ARC Small Grant (2001) at Griffith University.

References

[1] Foda MA, Chang J, Law A. Wave-induced breakout of half-buried marine pipes. J Waterways, Port, Coastal Ocean Engng, ASCE 1990; 116:267–86.
[2] Wagner DA, Murff JD, Brennodden H, Sveggen O. Pipe–soil interaction model. The Eighth Offshore Technical Conference, paper 5504; 1987.
[3] Brennodden H, Lieng JT, Sotberg T, Verley RLP. An energy-based pipe-soil interaction model. The 10th Offshore Technical Conference, paper 6057; 1989.
[4] Allen DW, Lammert WF, Hale JR, Jacobsen V. Submarine pipeline on-bottom stability: recent AGA research. The 10th Offshore Technical Conference, paper 6055; 1989.
[5] Lawlor CDF, Flynn SJA. Subsea pipeline stability analysis: still a black art? Trans Inst Engrs, Aust: Civil Engng 1991;33:1–8.
[6] Stansby PK, Starr P. On a horizontal cylinder resting on a sand bed under waves and currents. Int J Offshore Polar Engng 1992;2:262–6.
[7] Chakrabarti K. Offshore structure modeling. Singapore: World Scientific; 1994.
[8] Sumer BM, Fredsoe J. Onset of scour below a pipeline exposed to waves. Int J Offshore Polar Engng 1991;1:189–94.
[9] Poorooshasb F. On centrifuge use for ocean research. Mar Geotechnol 1990;9:141–58.